Journal of Biomedical Materials Research Part A

WILEY

Society For Biomaterials

RESEARCH ARTICLE

Influence of Diol Chain Length on Various Properties of Citric Acid Polyesters/PLA Electrospun Nonwovens for Tissue Engineering Applications

Aleksandra Bandzerewicz[1] | Adrian Chlanda[2] | Tomasz Gołofit[1] | Miroslav Slouf[3] | Piotr Denis[4] | Agnieszka Gadomska-Gajadhur[1]

[1]Faculty of Chemistry, Warsaw University of Technology, Warsaw, Poland | [2]Łukasiewicz Research Network – Institute of Microelectronics and Photonics, Flake Graphene Research Group, Warsaw, Poland | [3]Institute of Macromolecular Chemistry, Czech Academy of Sciences, Prague, Czech Republic | [4]Laboratory of Polymers and Biomaterials, Institute of Fundamental Technological Research, Polish Academy of Sciences, Warsaw, Poland

Correspondence: Agnieszka Gadomska-Gajadhur (agnieszka.gajadhur@pw.edu.pl)

Received: 18 March 2025 | **Revised:** 4 June 2025 | **Accepted:** 8 July 2025

Funding: This work was supported by Politechnika Warszawska.

Keywords: electrospinning | nonwovens | poly(diol citrates) | tissue engineering

ABSTRACT

Despite the great potential of citrate polyesters in regenerative medicine, the data about their application in electrospinning is somewhat limited. In this work, poly(dimethylene citrate) (P-1,2-ECit), poly(tetramethylene citrate) (P-1,4-BCit), and poly(hexamethylene citrate) (P-1,6-HCit) were synthesized. Nonwovens from poly(diol citrates)/PLA mixtures were successfully electrospun and characterized using SEM, AFM, water contact angle measurement, DSC, TGA, and in vitro degradation tests. The addition of poly(diol citrates) increases the hydrophilicity and surface adhesion force of PLA nonwovens; however, the observed effects depend on the scale level (macro/micro) of the analysis. Diol chain length in poly(diol citrate) influences the compatibility and heterogeneity of its distribution within the carrier polymer. Additionally, it impacts the crystallinity of the PLA phase. Degradation tests show the problem of the nonwoven stability in the aqueous media and the high leachability of the short-chained poly(diol citrates). Addressing this issue is important regarding controlling the degradation kinetics. Despite the good processability in electrospinning and promising surface properties of the poly(diol citrates)/PLA mixtures, the instability of these materials in an aqueous environment is an important issue which can subsequently affect the performance of the eventual implant/cell scaffold. The solution may involve chain elongation of the hydrophilic oligomeric additive.

1 | Introduction

The primary treatment of obstructed or narrowed blood vessels is by vascular bypass with autogenous material. The method is highly invasive and remains a high-risk operation despite the continuous development of medical knowledge. The risk of complications depends on the patient's general health and increases in elderly patients and/or those burdened with comorbidities [1–4]. Admittedly, a significant advantage of this type of surgery is the immediate availability of autologous vessels. Native vascular tissue has the biological and structural properties for optimal graft performance. However, up to one-third of patients with peripheral artery disease do not have suitable vessels for autologous transplantation [5, 6], hence a different approach is needed to address this challenge.

Synthetic vascular prostheses, shaped like tubes, offer an alternative to transplanting fully formed blood vessels. Several types have been introduced into clinical practice, including dacron (PET) and polytetrafluoroethylene (PTFE). The main limitation

of those prostheses is the increased thrombogenicity and the subsequent difficulty of maintaining long-term patency. This is particularly concerning for small-diameter prostheses (< 6 mm) [5–11]. This motivated us to look for new solutions in order to overcome this drawback.

The intensive development of tissue engineering offers promising prospects for innovative tissue regeneration. The premise is to support tissue regeneration with an artificial scaffold. The synthetic implant is temporary, and natural tissue should be rebuilt in its place [6, 12–15]. Many potential synthetic grafts are produced by electrospinning—a process that typically produces a structure with appropriate architecture and pores size [16–21]. It is also possible to create cylindrical structures: tissue-engineered vascular grafts (TEVG) [22, 23]. Despite advancements in manufacturing such implants and improvements in cell harvesting, multiplication, and incorporation, commercially available products and ongoing clinical trials are limited to TEVG with diameters > 6 mm [17, 22, 24]. It is worth underlining that the aforementioned limitation is regardless of the type of material from which TEVG is manufactured.

There is a group of the best-known polymers for tissue engineering applications, including polylactide, polyglycolide, poly(lactide-co-glycolide), polycaprolactone, or poly(glycerol sebacate) [25–31]. However, the research interest in this polyester type is growing, and a broader range of materials is being studied. Among them is a family of biodegradable and elastomeric poly(diol citrates). The primary representative of this group of polyesters is poly(octamethylene citrate) (POC). POC has been known in the literature for more than 20 years and is considered for manufacturing small blood vessel substitutes [32–35]. Other diols than 1,8-octanediol can be used to synthesize similar polyesters, although it impacts their mechanical properties and degradability [32, 36]. Despite its promising results in biocompatibility, POC on its own is somewhat problematic for the electrospinning procedure. The molecular weight of the uncrosslinked prepolymer needs to be higher to ensure the continuity of the solution stream during electrospinning. It is not possible to generate the necessary chain entanglement. On the other hand, the lack of solubility excludes the use of gelled (crosslinked) POC [37–40]. A popular solution to this problem is to use another spinnable polymer as a carrier—most commonly polylactide, poly(ε-caprolactone), or their copolymers. The carrier polymer then plays a structure-forming role as a scaffold for the polycitrate. Nonwovens obtained from such blends have different mechanical and surface properties compared to the carrier polymer; typically, the elasticity and hydrophilicity of the material increase while the degradation time is reduced. Improving the surface properties of the carrier polymer, especially in terms of hydrophilicity, is an essential aspect of cell scaffolds, as it can regulate cell adhesion and proliferation on their surface [40–47].

It is well established that the properties of the electrospun nonwovens depend on various parameters, including the type of solvent, the concentration of the solution, the applied voltage, etc. An important observation in this research topic is the lack of compatibility of POC with polylactide, resulting in a separation into a continuous PLA phase and POC dispersed in it. According to model calculations, the area of compatibility between POC and PLA should fall between a POC mass content of less than 25.5% and more than 70% [40, 48–51]. The possible incompatibility is related to the linear and branched structure of the two polymers and the difference in their polarity [40, 48]. As a result, the addition of polycitrate only sometimes provides the fiber mats with increased hydrophilicity, which depends not only on the composition of the spinning mixture but also on the distribution of its components on the surface of the nonwovens. In that case, the influence of the continuous phase is more significant than that of the dispersed phase [40, 52]. However, considerable data indicate a hydrophilizing effect of adding POC to the carrier polymer [41, 48, 53, 54]. It is possible that the discrepancies described are the result of randomness in the arrangement of the polymers in the fibers [55].

Despite auspicious results regarding the use of citrate polymers in regenerative medicine, data on the use of POC in electrospinning is relatively limited, and even more so for other such polyesters. The results between the different works are oftentimes somewhat inconsistent. In particular, the stability of such a system of two polymers, one of which is a much smaller and highly branched molecule and the other, the carrier polymer, is long and linear, is a rarely addressed issue, especially about the durability of nonwovens in aqueous environments [38, 40–44, 48, 53, 56, 57].

In this work, three different poly(diol citrates) were synthesized and mixed with PLA to electrospin nonwovens. The diol monomers differed in the length of the aliphatic chain. The objective was to study and compare the influence of aliphatic chain length on the properties of nonwovens, with particular emphasis on their surface properties and durability in an aqueous medium. This is a particularly important aspect of the characterization of biomaterials for in vivo tissue reconstruction. However, there is a shortage of available literature on the subject of poly(diols citrate) nonwovens, particularly comparative studies concerning different diols. Therefore, in this paper we seek to address these shortcomings by providing an in-depth analysis of the effects of the components of electrospun nonwovens on the major structural, surface, and thermal properties and the stability in an aqueous environment.

2 | Results and Discussion

2.1 | Electrospinning of the Nonwovens

Poly(dimethylene citrate) (P-1,2-ECit), poly(tetramethylene citrate) (P-1,4-BCit), and poly(hexamethylene citrate) (P-1,6-HCit) were obtained via simple polycondensation (Figure 1).

Following the literature data, a typical spinnable carrier polymer, polylactide, was used in mixtures with the poly(diol citrates) (mass ratio 50:50). Nonwovens were electrospun as thin (< 1 mm thick) sheets. The fibrous structure of the materials was confirmed by SEM micrographs (Figure 2).

Despite the relatively high poly(diol citrates) content, generally well-formed fibers with diameters of approximately 0.5–2 μm were obtained in all cases. Few structural defects in the form of beads, twists, bends, and locally flattened, not fully formed

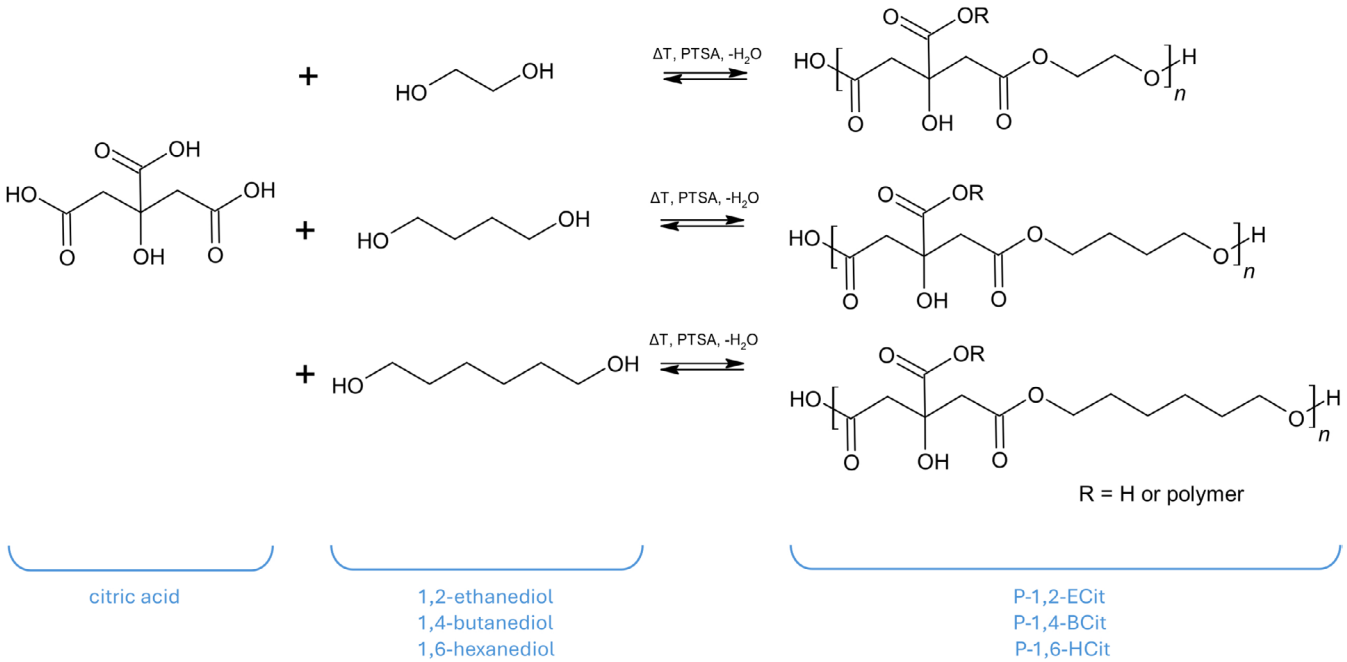

FIGURE 1 | Schematic illustration of the synthesis of poly(dimethylene citrate), poly(tetramethylene citrate), and poly(hexamethylene citrate).

fibers are visible for all types of spun nonwovens (particularly with the addition of poly(diol citrates) with the shorter aliphatic diol chain, namely P-1,2-ECit and P-1,4-BCit).

Based on SEM imaging, fibers from PLA without any additive appear to be more homogeneous in terms of formation quality and diameter. However, it does not seem as if the addition of poly(diol citrates) substantially affected the quality of the fiber structure. The fiber orientation is somewhat disordered and random, which is a typical characteristic in the case of fibers deposited on a drum collector with a slow rotational speed (like in this study).

2.2 | Surface Analysis

The hydrophilicity of the nonwoven surfaces was measured by determining the water contact angle. The wetting angle of the polycitrate resins used for electrospinning was also determined as a reference. The results are presented in Table 1.

One of the reasons for using citric acid and short-chain diols is to obtain hydrophilic polymers, the addition of which should improve the water wettability of PLA nonwovens. As evidenced by the measurements of the resins, hydrophilic materials were indeed obtained. At the same time, differences in aliphatic chain lengths do not seem to affect the results, as there is no actual change between P-1,2-ECit, P-1,4-ECit, and P-1,6-HCit.

The measurements were conducted as soon as the droplet was placed on the surface, but it should be noted that the water soaked into the material very quickly. Due to the high content of hydrophilic groups, especially on the surface, the amount of methylene groups in the diol molecule does not necessarily play a significant role in this particular case. Nonwovens made from PLA have a contact angle of approximately 120°, which is in accordance with literature values [40, 58, 59]. The addition of polycitrates causes the contact angle to drop below 90°, making the nonwoven surfaces hydrophilic. However, the pattern of changes in hydrophilicity is unexpected—the wettability of the surface increases with the lengthening of the diol chain in the polycitrate. The P-1,6-HCit/PLA nonwoven showed the highest water wettability in the test—the droplet dissolved as soon as it was placed and soaked into the material, making measurement impossible. In the case of the PLA nonwovens, no water soaking occurred even after extended observation times.

The differences in water contact angle between the three poly(diol citrate) resins are negligibly slight and do not correlate with the effect observed for nonwovens. This indicates that the described changes in surface hydrophilicity are not simply due to the presence of the poly(diol citrate) in the electrospinning mixture but are the result of a more complex effect of the additive on the spun fibers. SEM micrographs showed no noticeable differences in the morphology of the nonwovens, that is, areas of solid material, significant changes in fiber thickness or pore size, which could affect the result of the contact angle measurement. It is reasonable that the spatial organization of the constituent polymer chains in the fibers is essential.

Additional measurements of the surface of the nonwovens were carried out using atomic force microscopy (AFM). The results are presented as 2D and 3D topography maps (Figure 3) and adhesion force maps (Figure 4). The quantitative results of the adhesion forces are summarized in Table 2.

Based on the topographic images, it can be concluded that the microscale morphology of the nonwovens is similar between samples. All the images depicted a smooth surface of the fibers. Qualitative analysis of the 3D maps shows that irrespective of

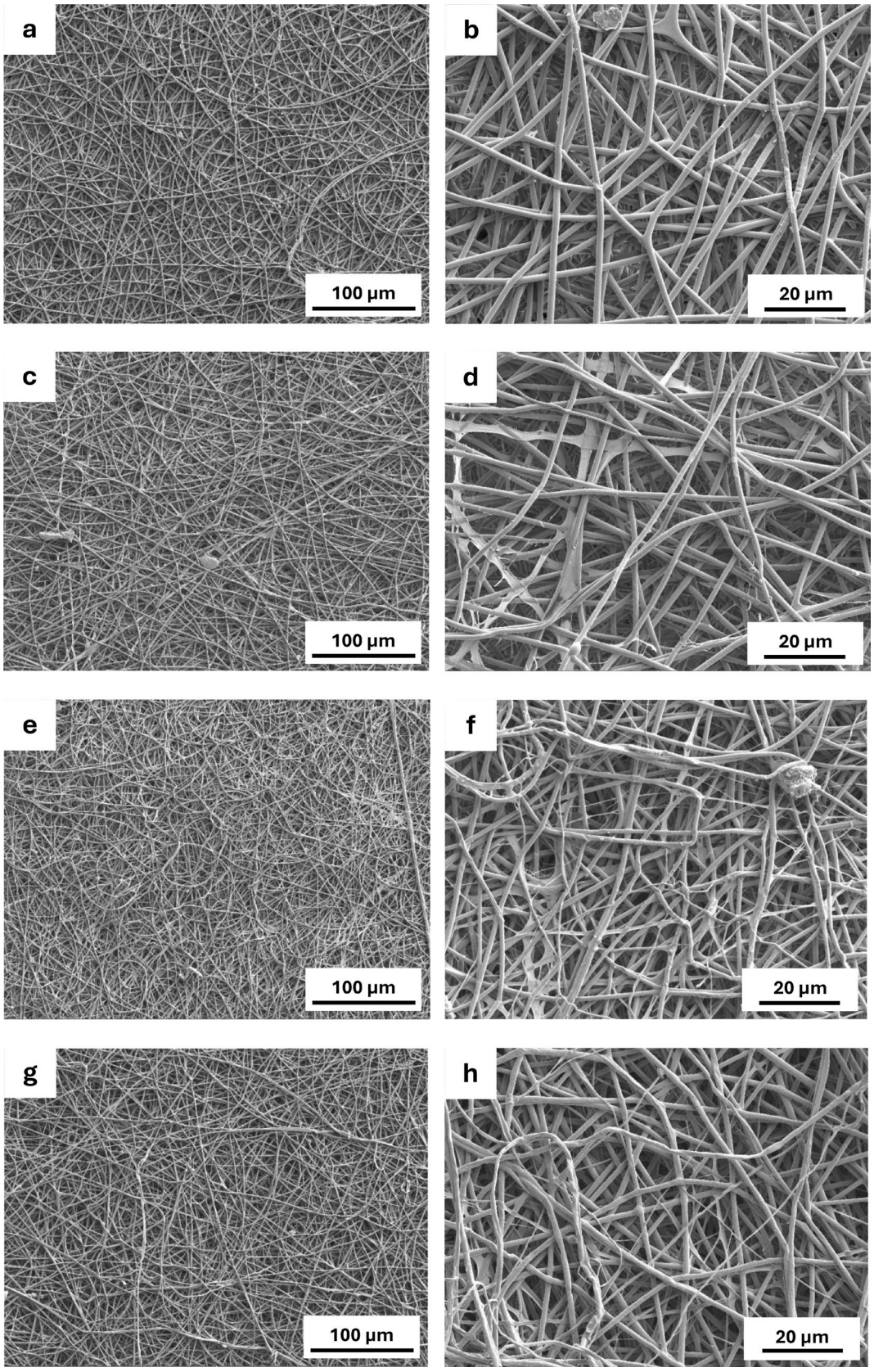

FIGURE 2 | SEM micrographs showing the morphology of electrospun nonwovens; from the top: PLA (a and b), P-1,2-ECit/PLA (c and d), P-1,4-BCit/PLA (e and f) and P-1,6-HCit/PLA (g and h).

the type of material studied, homogeneous, continuous fibers were obtained, with no thickening, thinning, or pores on the surface. The results support and complement the SEM micrograph analysis.

TABLE 1 | Results of water contact angle measurements of the nonwovens.

Material		Water contact angle [°]
Resin	P-1,2-ECit	23.5 ± 2.4
	P-1,4-BCit	24.4 ± 3.3
	P-1,6-HCit	24.5 ± 2.9
Nonwoven	PLA	118.5 ± 4.3
	P-1,2-ECit/PLA	85.7 ± 3.0
	P-1,4-BCit/PLA	54.9 ± 1.0
	P-1,6-HCit/PLA	The droplet spreads and soaks into the material

Note: Data show mean ± SD ($n = 3$).

The adhesion force maps and the numerical results vary between materials. The values obtained for the PLA nonwoven are relatively low, with the distribution of adhesion forces being uniform within the tested fiber (Figure 4a), as is the case for the P-1,6-HCit/PLA nonwoven (relatively uniform areas depicted in the map, Figure 4d). On the other hand, the maps for P-1,2-ECit/PLA and P-1,4-BCit/PLA materials are of particular interest. The alternation of light and dark areas (higher and lower adhesion, respectively) indicates a structural-related change [60, 61], which was followed by variations in the surface adhesion forces. This is reflected in the large scatter of the recorded numerical values (Table 2). The effect of the addition of hydrophilic poly(diol citrates) to the PLA carrier polymer is visible in the increase in fiber surface adhesion force values. However, the course of change is opposite (decrease in mean adhesion force) to that of the wetting angle, where a progressive increase in hydrophilicity from P-1,2-ECit/PLA to P-1,6-HCit/PLA was shown.

From the results of both analyses, one basic conclusion emerges: the observed effects and material surface properties are dependent on the level of structure (macroscopic/microscale/nanoscale approach). Poly(dimethylene citrate) (P-1,2-ECit) blended with polylactide causes the most remarkable changes in local fiber surface properties, but due to its shortest carbon chain and least compatibility with the carrier polymer, its concentration on the fiber surface is lower and more heterogeneous over a given area than that of poly(hexamethylene citrate) (P-1,6-HCit). As a result, the hydrophilicity of the surface understood in a macroscopic way (water contact angle) non-intuitively increases inversely to the assumptions (predominance of the resultant "macro" effect). The key question, therefore, is at what level of contact with the surface the application properties of the material should be considered.

2.3 | Thermal Analysis

Thermal analysis of poly(diol citrates) resins and nonwovens was performed using differential scanning calorimetry (DSC). Thermograms of the P-1,2-ECit, P-1,4-BCit, and P-1,6-HCit resins are shown in Figure 5.

The DSC curves of the first and second heating cycles illustrate the glass transition in the polymers, with the values of the glass transition temperatures T_g of a given poly(diol citrate) varying from cycle to cycle (areas A and E in Figure 5, respectively). The glass transition temperatures, as read from the cooling cycle curves (area D), correspond to the values in area E. The T_g values are summarized in Table 3.

The difference in T_g values between areas A and D/E is a consequence of the gelling of the resins during measurement. Gelation is additionally evident in the presence of a broad area B of the endothermic transition (> 110°C), showing the esterification of free COOH and OH groups and evaporation of the resulting water.

The significant increase in T_g values after gelling results from reduced mobility of the polymer chains and increased rigidity of the cross-linked, branched structure. In turn, the visibly different T_g values between individual poly(diol citrates) both before and after crosslinking are due to (1) differences in ester bond density per unit volume (P-1,2-ECit > P-1,4-BCit > P-1,6-HCit) due to the different number of methylene units in the diol monomers and (2) the strength of intermolecular hydrogen bonds. Higher bond density and strong hydrogen bonds between the free COOH and OH groups limit the mobility of the chains, leading to an increase in the glass transition temperature. The decrease in density with lengthening of the aliphatic diol chain is explained by the rise in inter-chain free volume between cross-links [36]. No signals from the crystallization or melting of poly(diol citrates) were observed.

The curve of the first heating cycle of P-1,4-BCit additionally shows a small endothermic C signal, stretching between about 50°C and 110°C. One possible explanation for this observation is the evaporation of THF formed during the synthesis reaction and bound in the resin. The reaction conditions, that is, elevated temperature and acidic environment, favor the cyclo-dehydration of 1,4-butanediol to THF. Admittedly, the boiling point of pure THF is 66°C, while it is possible that the dense arrangement of the polymer chains hinders its evaporation. On the basis of thermogravimetric analysis (TGA), it was determined that the weight loss of the resins from room temperature to 200°C is approximately 8%–11% (Figure 6). The changes in mass may be due to the evaporation of water formed during (1) the gelling of the polymer during analysis, and (2) synthesis in the reactor and bound in the resin structure (incomplete removal into the Dean-Stark apparatus). In the case of P-1,4-BCit, part of the recorded mass loss may be due to THF evaporation.

In the next step, a thermal analysis of the nonwovens was performed. A thermogram is shown in Figure 7, displaying the DSC curves.

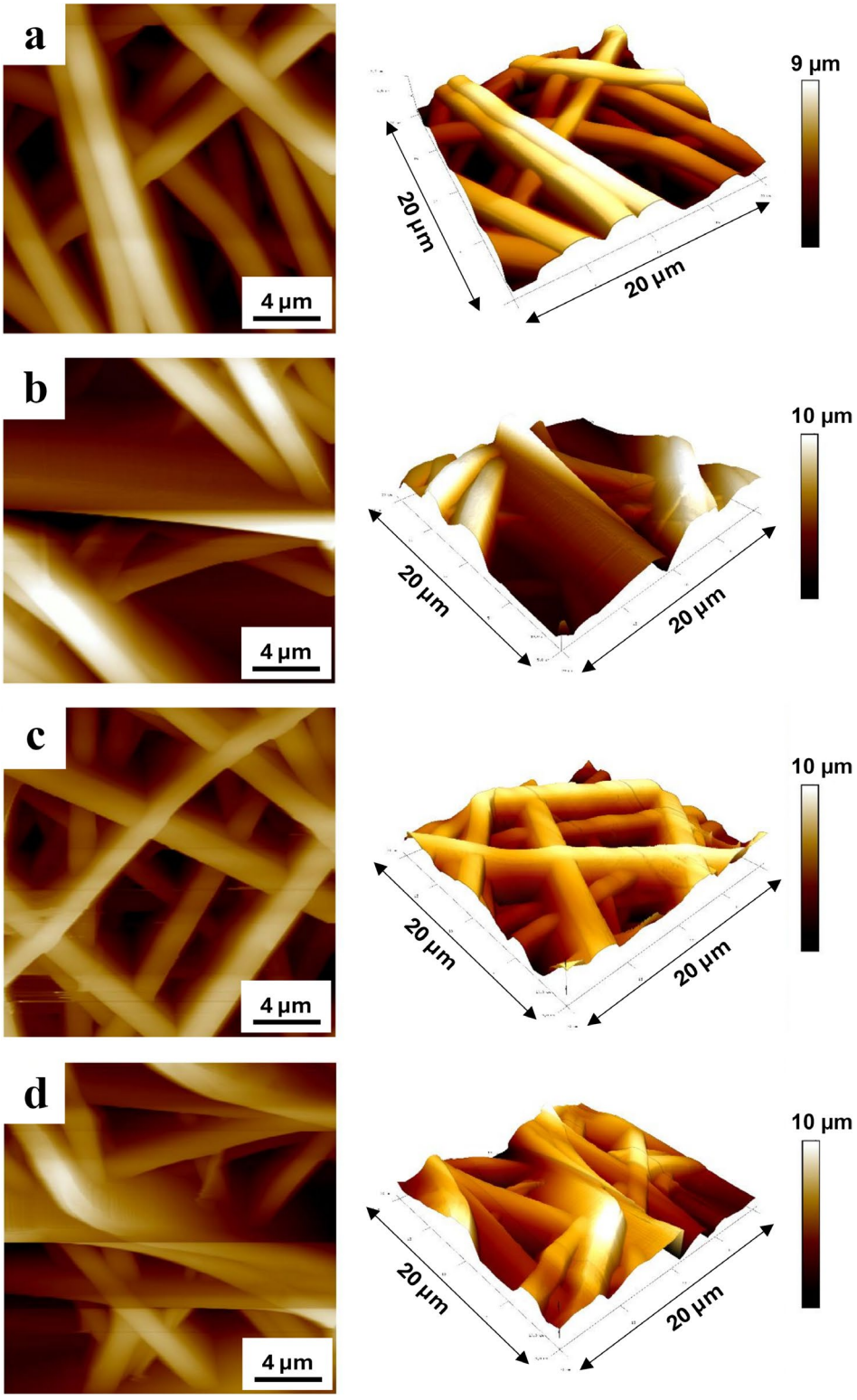

FIGURE 3 | 2D (left column) and 3D (right column) topographic images of nonwovens obtained by AFM; from the top: PLA (a), P-1,2-ECit/PLA (b), P-1,4-BCit/PLA (c), and P-1,6-HCit/PLA (d).

In the case of the PLA nonwoven, a glass transition temperature T_g (area F, Figure 7) of about 56°C and a melting temperature T_m (area H; peak maximum value is given) of about 186.5°C were observed. In addition, around 69.5°C, a process of crystallization of the amorphous fraction, the so-called "cold crystallization" (T_{cc}, area G), occurred, resulting from an increase in the mobility of the polymer chains at temperatures above T_g [62, 63]. The broadening of the endothermic melting signal G is due to some inhomogeneity of the polylactide in the nonwoven.

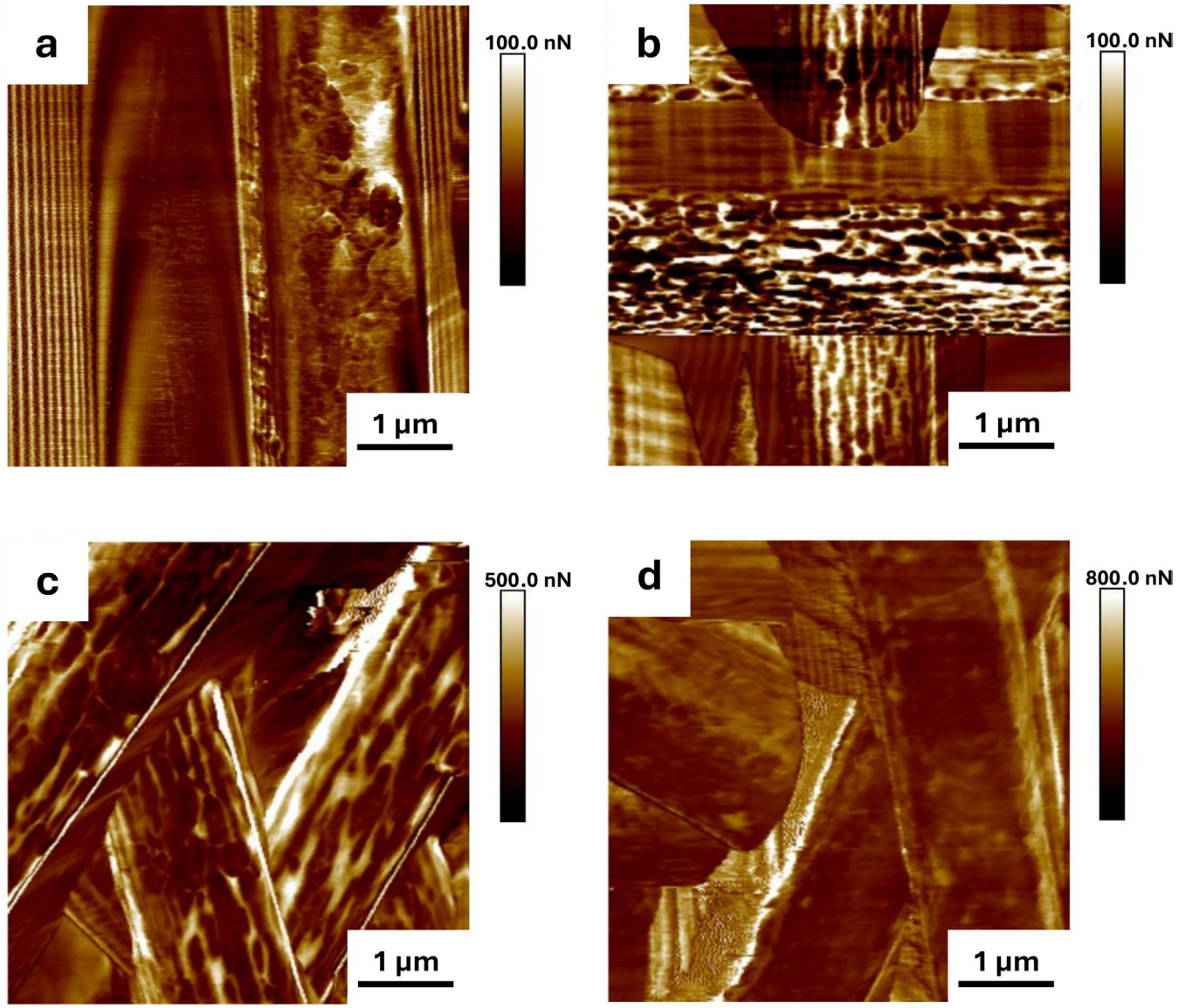

FIGURE 4 | Adhesion force maps of nonwovens obtained by AFM; from the top left: PLA (a), P-1,2-ECit/PLA (b), P-1,4-BCit/PLA (c), and P-1,6-HCit/PLA (d).

TABLE 2 | Results of adhesion force measurements (AFM).

Nonwoven	Adhesion force [nN]
PLA	17.0 ± 3
P-1,2-ECit/PLA	230.7 ± 68
P-1,4-BCit/PLA	191.6 ± 84
P-1,6-HCit/PLA	93.6 ± 20

Note: Data show mean ± SD ($n = 3$).

The influence of poly(diol citrates) is evident in the shift in characteristic temperatures of the polylactide, as shown in Table 4. The values of T_g, T_{cc}, and T_m are dependent on a number of factors, including intermolecular interactions, steric effects, chain flexibility, molecular weight, or cross-linking density. The addition of short-chain poly(diol citrates) disrupts the continuity of the polylactide phase and results in a reduction of the PLA crystalline phase content. A reduction in the cold crystallization process of the amorphous phase is also observed (based on the decreasing value of ΔH_{cc}), which is probably related to the reduction in the number of crystallization nuclei and their limited growth due to the presence of the oligomeric additive. This means that poly(diol citrates) do not act as nucleating agents for the PLA crystallization process. Furthermore, they reduce the mobility of PLA chains, as indicated by an increase in T_g and T_{cc} temperatures.

The DSC curve of the first heating cycle (Figure 7, left side) illustrates properties of the sample that depend on its manufacture, storage, and preparation (e.g., the presence of crystalline structures formed due to some mechanical pressure), which can interfere with the repeatability of the analysis run and cause a shift in characteristic temperatures. For this reason, it is common practice to remove the thermomechanical history of the sample by heating under measurement conditions and, thus—to carry out the actual analysis on the basis of a second heating cycle. In the present case, the interpretation of the first measurement curve

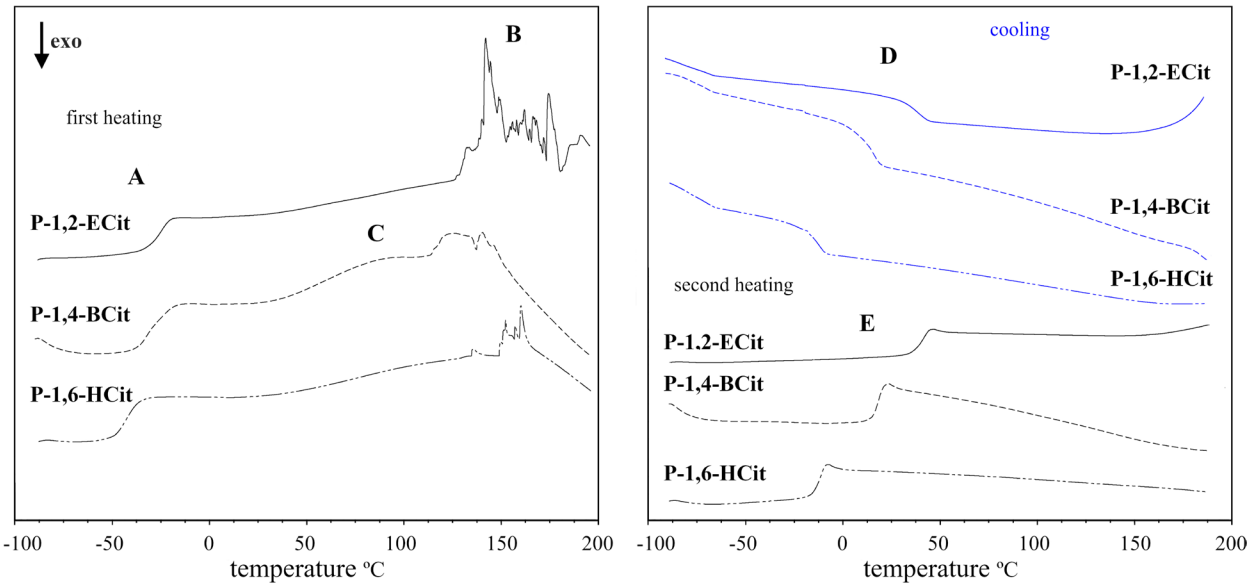

FIGURE 5 | DSC curves from the first and second heating cycle (black lines) and the cooling cycle (blue) obtained for P-1,2-ECit, P-1,4-BCit, and P-1,6-HCit resins. Measurements were carried out at a temperature change rate of 10°C/min.

TABLE 3 | Glass transition temperatures of poly(diol citrates) before and after gelling.

	Glass transition temperature [°C]	
Resin	T_g **(A)**	T_g **(D, E)**
P-1,2-ECit	−23.1	43.6
P-1,4-BCit	−26.9	20.3
P-1,6-HCit	−40.6	−8.4

is intentional and is based on the assumption of further application of the tested materials. Potential vascular implants would go into use immediately after manufacture and sterilization, so the thermomechanical history would have an impact on their performance.

In order to determine the effect of the first heating cycle on the thermal properties of the nonwovens, an additional analysis of the cooling and second heating curves was performed (Figure 7, right side). During the cooling, a broad exothermic crystallization peak of PLA is observed (area I; maximum at 100.2°C–120.9°C). The discrepancies are due to the quality of the crystal formation, which is influenced by the presence of poly(diol citrates). The width and (in some cases) bimodality of the peak can be related to the cooling rate, among other factors.

Also visible are signals corresponding to the glass transitions of PLA (J; 58.4°C) and the poly(diol citrates): P-1,4-BCit (K; 16.6°C) and P-1,6-HCit (L; −8.7°C); the glass transition of P-1,2-ECit overlaps with PLA, giving a single signal in area J. Values J, K, and L correspond to areas M, P, and R, respectively. The T_g temperatures of the poly(diol citrates) indicate that cross-linking has occurred.

The intensity of the heat flow in the cold crystallization area of PLA during the second heating (N) is noticeably lower than during the first cycle (G) or the cooling (I). The T_{cc} temperature of I/N is also significantly higher than that of G, which may be related to the formation of a cross-linked polycitrate structure that limits the mobility of the PLA chains. No significant change in PLA melting temperatures was observed in the nonwovens (area O; maximum at 178.9°C–181.5°C) between the two heating cycles.

2.4 | In Vitro Degradation Tests

The stability of the nonwovens in an aqueous environment was investigated as the course of degradation (material weight loss) in PBS buffer (37°C) at given time intervals. The PBS buffer is the most commonly used fluid to simulate in vivo conditions, suggested by the international standard ISO 10993-13:2010 as suitable for the in vitro assessment of polymeric material degradation (despite the absence of relevant body environment factors, i.e., exposure to mechanical stresses, immune response cells, enzymes, etc.).

The results are shown in Figure 8A as a percentage of the initial weight of the nonwoven: the 50% limit, that is, the mass content of poly(diol citrate) in the electrospinning mixture, was marked. Changes in the pH value of the buffer over time were investigated. The example of the degrading effect of the aqueous environment on the morphology of the nonwovens is shown in SEM micrographs (Figure 8B).

The results presented here demonstrate the existing problem of the incompatibility of polylactide with nonlinear polymers of higher hydrophilicity and much lower molecular weight. The majority of poly(diol citrate) leaches out of the material after the first day. It is likely that the lack of a clear trend in the degradation pattern of one type of nonwoven and the variation between nonwovens containing different poly(diol citrate) is more a result of the uneven distribution of the component polymers in the material rather than the actual effect of the aliphatic chain

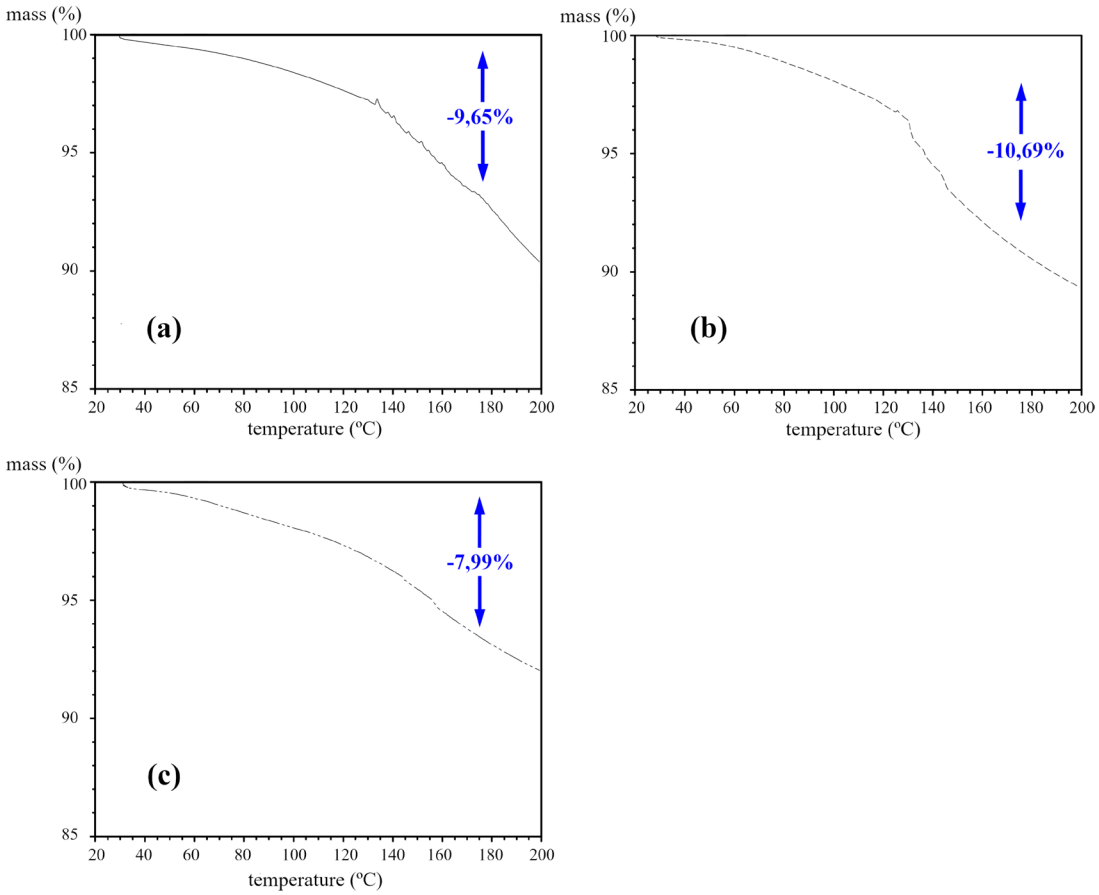

FIGURE 6 | TGA curves obtained for P-1,2-ECit (a), P-1,4-BCit (b), and P-1,6-HCit (c) resins.

length of the diol on the stability of these materials in an aqueous environment. It is especially visible in the inconsistency of the P-1,4-BCit/PLA nonwoven degradation pattern, where little difference can be distinguished between the 1st and 14th days of the degradation test despite some fluctuations in between.

Poly(diol citrate) will leach much faster from the outer layers, where contact with the degrading medium is greater. It is, however, possible that the greater homogeneity of the polymer distribution on the fiber surface of P-1,6-HCit/PLA compared to P-1,2-ECit/PLA and P-1,4-BCit/PLA influences the consistent level of weight loss over the time interval studied.

The morphology of the PLA nonwoven did not visibly change after 14 days in the degradation medium. In the case of the nonwoven containing P-1,4-BCit, there is a clearly visible thinning of the fibers, indicating washing the surface layer out while maintaining the porous fiber structure. The undegraded residue is the polylactide core of the nonwoven fabric. SEM micrographs for the presented material (Figure 8B) and two other nonwovens confirm the results of the mass change measurements.

The decrease in the pH value of the PBS buffer is due to the presence of washed-out poly(diol citrate) molecules, which contain free carboxyl groups. The macromolecules then hydrolyze to shorter oligoesters until the ester bonds are completely broken down into monomers. Cross-linked poly(diols citrate) films degrade completely after about 60–90 days under conditions similar to those described in this work, with a clear synergistic effect of the aqueous environment and the acidic properties of the material (autocatalysis) on the hydrolysis of the ester bonds [55]. A 50% mass addition of PLA in nonwovens reduces the acidification of the medium by the degrading polycitrate fraction.

In the case of the PLA nonwovens, no weight loss or acidification of the medium was observed due to the significantly longer degradation time of PLA than the time of the analysis. However, due to the conclusions described above, continuing the study beyond 14 days was considered unreasonable.

According to studies [55, 64], nonwoven fabrics made of mixtures of polylactide with citric acid polyesters and short-chain diols do not show toxicity toward cells; it is possible to maintain a cell culture on the surface. The decrease in cell viability after a certain time is attributed to a reduced growth area and nutrient depletion rather than to the toxic effect of poly(diol citrate). It remains an open question as to whether the observed growth of cells on the nonwoven fabric is not simply a result of the contact with mainly polylactide following the rapid washing out of poly(diol citrate) in contact with an aqueous medium. Nevertheless, even assuming this, no cytotoxic effect of leached and hydrolysable poly(diol citrate) in the culture medium is observed. This indicates the potential of poly(diol citrates) in the role of biomaterials while highlighting the problem of durability of nonwovens obtained from typical electrospinning mixtures.

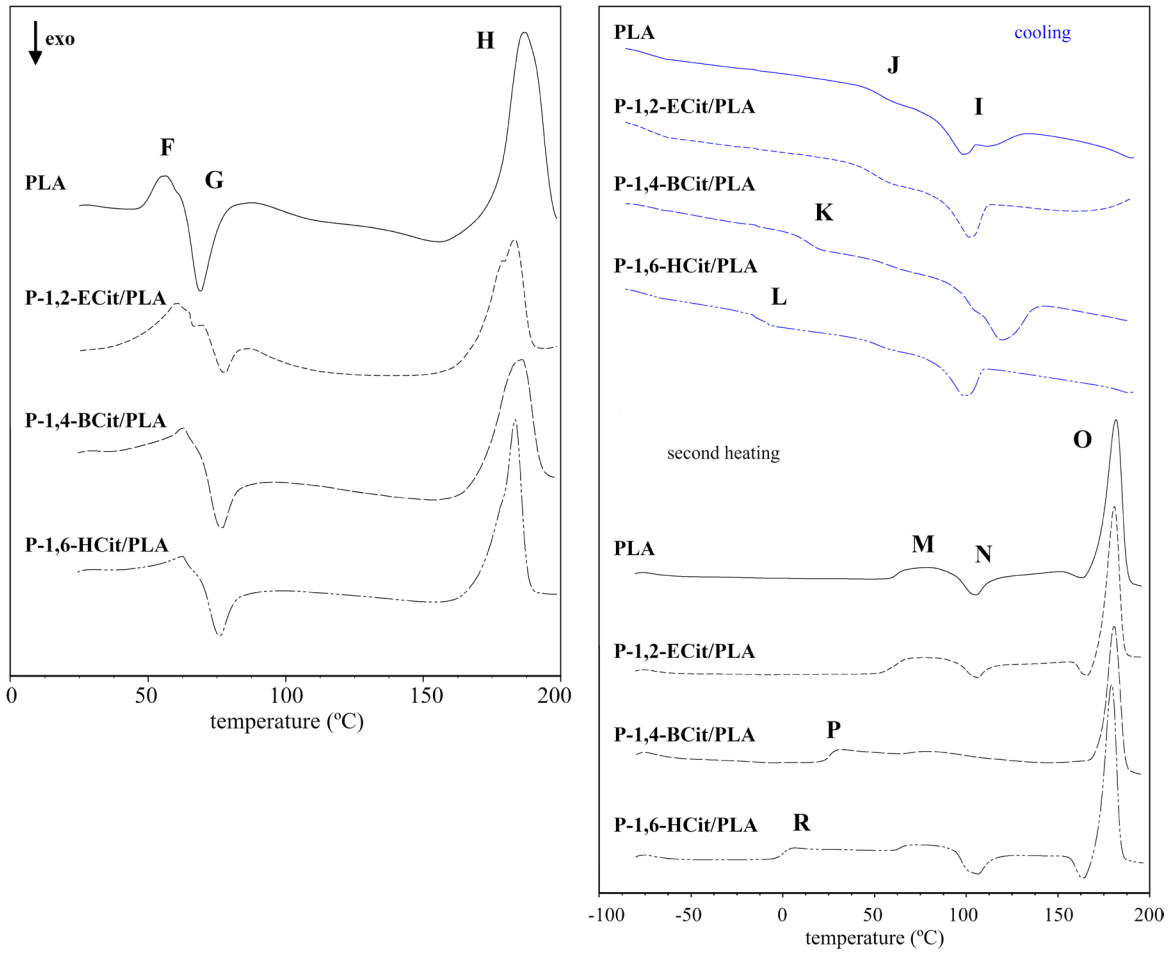

FIGURE 7 | DSC curves from measurements obtained for nonwovens made of PLA and poly(diol citrates)/PLA blends: on the left side—the first heating cycle, on the right side—the cooling cycle (blue lines) and the second heating cycle (black). Measurements were carried out at a temperature change rate of 10°C/min.

TABLE 4 | Thermal characteristics of PLA and poly(diol citrates)/PLA nonwovens.

	Glass transition temperature [°C]					
Nonwoven	T_g (F)	T_{cc} (G)	T_m (H)	ΔH_{cc} [J/g]	ΔH_m [J/g]	X_c [%]
PLA	56.0	69.5	186.5	12.7	50.9	41.0
P-1,2-ECit/PLA	60.1	77.8	182.9	2.4	26.2	25.6
P-1,4-BCit/PLA	63.2	77.4	185.5	5.0	28.7	25.5
P-1,6-HCit/PLA	62.9	77.0	183.4	5.0	30.9	27.8

Abbreviations: ΔH_{cc}, enthalpy of cold crystallization of PLA in the nonwoven; ΔH_m, enthalpy of melting of PLA in the nonwoven; T_{cc}, cold crystallization temperature; T_g, glass transition temperature; T_m, melting temperature; X_c, degree of crystallinity of PLA in the nonwoven.

3 | Conclusion

The use of electrospinning is a common method for obtaining polymeric cell scaffolds, yet the most widely known and used spinnable polymers exhibit poor surface properties for cell adhesion. Hence, investigating various additives to improve these limitations is a popular research trend. This work demonstrated that the addition of highly hydrophilic polyesters based on citric acid and short-chain diols significantly affects the surface properties of nonwovens made from PLA, a typical spinnable/carrier polymer. Nevertheless, beyond the mere hydrophilicity of the polymers blended with PLA for electrospinning, the spatial organization of the chains in the fibers and the actual distribution and proportion of both polymers present within or near the surface levels have a significant impact on said properties. Poly(dimethylene citrate), despite causing the highest local changes in the surface adhesion force of a fiber, seems to be the least compatible with PLA

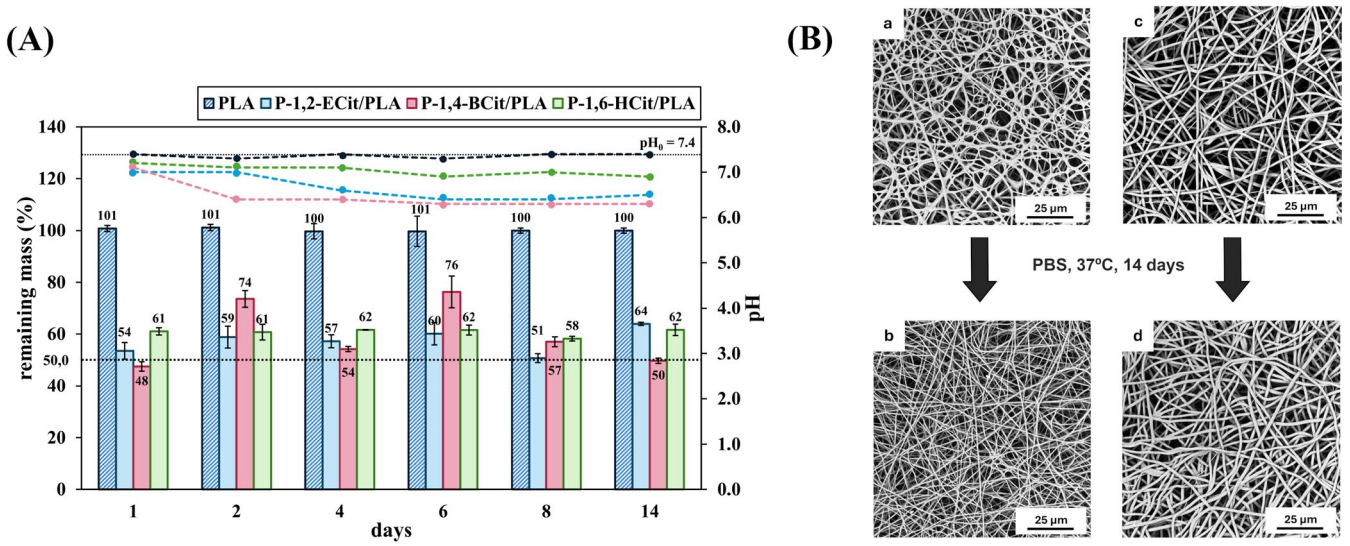

FIGURE 8 | Results of the in vitro degradation tests: (A) degradation of the PCit/PLA nonwovens in PBS buffer as percentage changes in sample weight relative to initial weight (bar graph); comparison with the degradation pattern of nonwovens from polylactide. The dashed lines represent changes in the pH value of the buffer over time; data show mean ± SD ($n = 3$); (B) SEM micrographs showing the morphology of nonwovens before and after 14-day degradation in PBS buffer; P-1,4-BCit/PLA (a and b) and PLA (c and d) nonwovens.

in terms of chain length, causing a more uneven distribution than poly(hexamethylene citrate). As a result, the hydrophilicity measured by water contact angle values increases along with the diol chain length because of the overall "macro" effect determined by the better compatibility and more homogenous mixing of both polymers.

This effect may not be such an issue itself, as the desired "level" of impact on surface properties can be tailor-made and adjusted for a given application, for example, the size of cells to be cultured on such a scaffold. However, the major limitation of such polymer mixtures, which consist of highly dissimilar components in terms of chain length, degree of branching, and hydrophilicity, is their instability in an aqueous environment, as is the case of presented poly(diol citrates)/PLA. Even a major improvement in surface properties is ultimately insignificant if one of the nonwoven components is washed away instantaneously. Even so, adequate degradation tests are relatively rare in published work in this field.

The results and issues described in this work are by no means an attempt to discourage research on similar topics but rather to draw attention to an important limitation of this type of electrospun materials. The authors suggest that one possible solution is to use hydrophilizing additives to PLA with a longer polymer chain, which would allow greater chain entanglement in the fiber and consequently reduce leaching. It is, however, impossible to obtain poly(citrate diols) with a higher molecular weight than used in this study due to the functionality of citric acid (three carboxyl groups), resulting in a branched polyester. Achieving a higher monomer conversion is not possible due to the gelation of the reaction mixture at the critical conversion point and the formation of an insoluble, unprocessable product. Therefore, the best approach seems to be a post-polymerization modification of the poly(diol citrates), for example, using other oligomers/polymers.

4 | Experimental Section/Methods

4.1 | Materials

1,2-Ethanediol (Fisher Chemical, ≥99%), 1,4-butanediol (Thermo Scientific, ≥99%), 1,6-hexanediol (Angene, ≥98%), anhydrous citric acid (Acros Organics, ≥99.5%), and p-toluenesulfonic acid monohydrate (PTSA; Sigma Aldrich, ≥98.5%) were used without prior preparation. For the preparation of the polymer solutions for electrospinning, poly-L-lactide Purasorb PL49 was purchased from Corbion (no longer available).

4.2 | Polymer Synthesis

The syntheses of polyesters were carried out in a Mettler Toledo MultiMax parallel reactors system; reactors were equipped with a mechanical stirrer, temperature sensor, and Dean-Stark apparatus. PTSA was added at 1% (w/w) relative to citric acid. The reaction mixture was heated for 10 min to a temperature of 130°C, which was then held constant for 30, 50, or 60 min, depending on the diol monomer.

4.3 | Electrospinning

Electrospinning was carried out using 1,1,1,3,3,3-hexafluoro-2-propanol (HFIP) as a solvent. A solution of the polymers, poly(diol citrates), and PLA (1:1 mass ratio) was prepared at a 5% mass concentration and left for stirring on a magnetic stirrer for 24 h at a rotation speed of 150 rpm.

A drum (rotary) collector with a diameter of 8 cm and a rotational speed of 250 rpm was used, with a distance between the needle tip and the collector surface of 14 cm and a solution feed rate of 1.5 mL/h. The spinning solution was fed using a 23G needle. The

value of the applied voltage was 10.5–12.0 kV. The nonwovens were dried after spinning to remove residual solvent.

4.4 | Scanning Electron Microscopy

The samples were attached to an aluminum base using a double-adhesive carbon tape and coated with a 4 nm thick platinum layer (SCD 050 vacuum sputtering machine; Leica, Vienna, Austria). The top side of the samples was observed using a MAIA 3 SEM microscope (TESCAN, Brno, Czech Republic). Micrographs were obtained using a secondary electron detector at an accelerating voltage of 3 kV.

4.5 | Water Contact Angle Measurement

Samples were prepared as follows: (1) the resins were heated to approximately 35°C; a small amount was spread evenly on a microscope slide and allowed to cool; (2) samples of approximately 1 cm × 1 cm were cut from the nonwovens with a scalpel and placed on a microscope slide.

The prepared samples were placed on a mobile table with a UCMOS01300KPA digital camera and a fixed microscope adapter FMA037. Drops of deionized water were deposited on the surface of the samples using a syringe with a needle. ToupView software was used to measure the wetting angle values. The results from five samples were averaged; the data was calculated as mean ± SD.

4.6 | AFM

The atomic force microscope (Dimension Icon, Bruker) was used to visualize the topography of nonwovens and to study the adhesion force between the scanning probe tip and the surface of the fibers. Imaging of the nonwovens was performed in tapping mode (TM), while the adhesion force study was conducted in quantitative nano mechanics (QNM) mode. For both studies, an ACST probe (AppNano) with a spring constant of approximately 7.8 N/m and a tip radius of curvature below 10 nm (data suggested by the manufacturer) was mounted in an Icon-type AFM scanning head. Both studies were carried out in air at room temperature (approximately 21°C). The samples were mounted on the microscope table and enclosed in a chamber (provided by the manufacturer) designed to protect the measurement system from acoustic disturbances. Topographic and QNM maps were acquired at 10 randomly selected locations on each material, and the obtained results were analyzed using the dedicated NanoScope Analysis software.

4.7 | Differential Scanning Calorimetry

Measurements were performed on a DSC Q2000 (TA Instruments) in an aluminum vessel in a nitrogen flow and at a constant temperature gradient of 10°C/min. The mass of the samples was 7–10 mg. A program in heating–cooling–heating mode was established. The degree of PLLA crystallinity in the nonwovens was calculated according to the formula:

$$X_c = \frac{\Delta H_m - \Delta H_{cc}}{\Delta H_m^0} \cdot 100\% \quad (1)$$

where X_c is the degree of crystallinity of PLLA in the nonwoven, ΔH_m the enthalpy of melting of PLLA in the nonwoven (J/g), ΔH_{cc} the enthalpy of cold crystallization of PLLA in the nonwoven (J/g), and ΔH_m^0 is the enthalpy of melting of fully crystallized PLLA equal to 93.1 J/g.

4.8 | TGA

Measurements were performed on an SDT Q600 analyzer (TA Instruments, Eschborn, Germany) in a nitrogen flow and at a constant temperature gradient of 10°C/min. The mass of the samples was 6–10 mg.

4.9 | In Vitro Degradation Tests

Discs with a diameter of 1.5 cm were cut from the materials and placed in 5 mL plastic tubes with a screw cap; 1.5 mL of freshly prepared PBS solution was poured into each tube. The tubes thus prepared were placed on a Heidolph reciprocating motion shaker equipped with a thermostatic chamber. A temperature of 37°C and a rotation speed of 50 rpm were maintained for a maximum of 14 days. After removal from the PBS, the discs were transferred to clean tubes, flooded with 5 mL of deionized water, and placed back on the shaker for 1 h to rinse any residual salt. The discs were then dried at room temperature under a vacuum (1 mbar) for 48 h. The weight loss at selected time points was determined according to the formula:

$$\text{remaining mass} = \frac{m_d}{m_0} \times 100\% \quad (2)$$

where m_0 is the mass of the sample before degradation and m_d is the mass of the dried sample after degradation. The results from the three tests were averaged. The data were calculated as mean ± SD.

4.10 | Statistical Analysis

All experiments were carried out as three independent experiments. Data were expressed as mean ± SD. All calculations were performed using Microsoft Excel software.

Acknowledgments

The research was funded by the Warsaw University of Technology within the Excellence Initiative: Research University (IDUB) program, a project called *Polyesters of azelaic acid and selected short-chain dihydroxy alcohols for the preparation of cell scaffolds*.

Conflicts of Interest

The authors declare that the research was conducted in the absence of any commercial or financial relationships that could be construed as a potential conflicts of interest.

Data Availability Statement

The data that support the findings of this study are available from the corresponding author upon reasonable request.

References

1. P. W. Serruys, M.-C. Morice, A. P. Kappetein, et al., "Percutaneous Coronary Intervention Versus Coronary-Artery Bypass Grafting for Severe Coronary Artery Disease," *New England Journal of Medicine* 360, no. 10 (2009): 961–972.

2. J. H. Alexander and P. K. Smith, "Coronary-Artery Bypass Grafting," *New England Journal of Medicine* 374, no. 20 (2016): 1954–1964.

3. T. Montrief, A. Koyfman, and B. Long, "Coronary Artery Bypass Graft Surgery Complications: A Review for Emergency Clinicians," *American Journal of Emergency Medicine* 36, no. 12 (2018): 2289–2297.

4. Y. Zhang, L. Lin, M. Niu, F. Bian, W. Wang, and Y. Zu, "Artificial Human Blood Vessels for Tissue Engineering," *ACS Materials Letters* 7, no. 4 (2025): 1626–1645.

5. S. Roll, J. Müller-Nordhorn, T. Keil, et al., "Dacron vs. PTFE as Bypass Materials in Peripheral Vascular Surgery – Systematic Review and Meta-Analysis," *BMC Surgery* 8, no. 1 (2008): 22.

6. S. Li, D. Sengupta, and S. Chien, "Vascular Tissue Engineering: From In Vitro to In Situ," *WIREs Systems Biology and Medicine* 6, no. 1 (2014): 61–76.

7. S. Vergnaud, V.-P. Riche, P. Tessier, N. Mauduit, A. Kaladji, and Y. Gouëffic, "Budget Impact Analysis of Heparin-Bonded Polytetrafluoroethylene Grafts (Propaten) Against Standard Polytetrafluoroethylene Grafts for Below-The-Knee Bypass in Patients With Critical Limb Ischaemia in France," *BMJ Open* 8, no. 2 (2018): e017320.

8. E. K. Gregory, A. Webb, J. M. Vercammen, et al., "Inhibiting Intimal Hyperplasia in Prosthetic Vascular Grafts via Immobilized All-Trans Retinoic Acid," *Journal of Controlled Release* 274 (2018): 69–80.

9. W. Hong, V. Tewari, H. Yu, J. Chen, and A. P. Sawchuk, "Evaluating Compliance in Three-Dimensional-Printed Polymeric Vascular Grafts Compared to Human Arteries and Commercial Grafts in a Mock Circulation Loop Compliance in Three-Dimensional-Printed Polymeric Vascular Grafts," *JVS-Vascular Science* 6 (2025): 100291.

10. M. Power Foley, N. Doolan, T. Connelly, and M. McMonagle, "Medium-Term Restenosis After Carotid Endarterectomy by Patch Type: A Single-Centre Retrospective Study Comparing Biological With Synthetic Patch Materials," *Annals of the Royal College of Surgeons of England* (2025).

11. S. Laroche, J. Danion, F. Perdigao, T. Baron, and E. Savier, "Migration of an Inferior Vena Cava Prosthesis Into the Duodenum (With Video)," *Surgery Open Digestive Advance* 18 (2025): 100209.

12. A. Wubneh, E. K. Tsekoura, C. Ayranci, and H. Uludağ, "Current State of Fabrication Technologies and Materials for Bone Tissue Engineering," *Acta Biomaterialia* 80 (2018): 1–30.

13. M. Eudy, C. L. Eudy, and S. Roy, "Apligraf as an Alternative to Skin Grafting in the Pediatric Population," *Cureus* 13, no. 7 (2021): e16226.

14. R. Langer and J. P. Vacanti, "Tissue Engineering," *Science* 260, no. 5110 (1993): 920–926.

15. X. Fu, J. Wang, D. Qian, et al., "Oxygen Atom-Concentrating Short Fibrous Sponge Regulates Cellular Respiration for Wound Healing," *Advanced Fiber Materials* 5, no. 5 (2023): 1773–1787.

16. L. R. Madden, D. J. Mortisen, E. M. Sussman, et al., "Proangiogenic Scaffolds as Functional Templates for Cardiac Tissue Engineering," *Proceedings of the National Academy of Sciences* 107, no. 34 (2010): 15211–15216.

17. K. M. Naegeli, M. H. Kural, Y. Li, J. Wang, E. A. Hugentobler, and L. E. Niklason, "Bioengineering Human Tissues and the Future of Vascular Replacement," *Circulation Research* 131, no. 1 (2022): 109–126.

18. Z. Liu, X. Liu, L. Bao, et al., "The Evaluation of Functional Small Intestinal Submucosa for Abdominal Wall Defect Repair in a Rat Model: Potent Effect of Sequential Release of VEGF and TGF-β1 on Host Integration," *Biomaterials* 276 (2021): 120999.

19. X. Fu, J. Wang, D. Qian, et al., "Living Electrospun Short Fibrous Sponge via Engineered Nanofat for Wound Healing," *Advanced Fiber Materials* 5, no. 3 (2023): 979–993.

20. Y. Xu, Q. Saiding, X. Zhou, J. Wang, W. Cui, and X. Chen, "Electrospun Fiber-Based Immune Engineering in Regenerative Medicine," *Smart Medicine* 3, no. 1 (2024): e20230034.

21. Y. Song, Q. Hu, S. Liu, et al., "Electrospinning/3D Printing Drug-Loaded Antibacterial Polycaprolactone Nanofiber/Sodium Alginate-Gelatin Hydrogel Bilayer Scaffold for Skin Wound Repair," *International Journal of Biological Macromolecules* 275 (2024): 129705.

22. P. Mallis, A. Kostakis, C. Stavropoulos-Giokas, and E. Michalopoulos, "Future Perspectives in Small-Diameter Vascular Graft Engineering," *Bioengineering* 7, no. 4 (2020): 160.

23. S. Ozdemir, J. Oztemur, H. Sezgin, and I. Yalcin-Enis, "Structural Design and Mechanical Analysis of Small-Caliber Bilayer Vascular Prostheses," *International Journal of Polymeric Materials and Polymeric Biomaterials* 74, no. 3 (2025): 181–191.

24. M. Carrabba and P. Madeddu, "Current Strategies for the Manufacture of Small Size Tissue Engineering Vascular Grafts," *Frontiers in Bioengineering and Biotechnology* 6 (2018): 41.

25. V. DeStefano, S. Khan, and A. Tabada, "Applications of PLA in Modern Medicine," *Engineered Regeneration* 1 (2020): 76–87.

26. Z. U. Arif, M. Y. Khalid, R. Noroozi, A. Sadeghianmaryan, M. Jalalvand, and M. Hossain, "Recent Advances in 3D-Printed Polylactide and Polycaprolactone-Based Biomaterials for Tissue Engineering Applications," *International Journal of Biological Macromolecules* 218 (2022): 930–968.

27. Q.-Z. Chen, A. Bismarck, U. Hansen, et al., "Characterisation of a Soft Elastomer Poly(Glycerol Sebacate) Designed to Match the Mechanical Properties of Myocardial Tissue," *Biomaterials* 29, no. 1 (2008): 47–57.

28. P. Yousefi Talouki, R. Tamimi, S. Zamanlui Benisi, et al., "Polyglycerol Sebacate (PGS)-Based Composite and Nanocomposites: Properties and Applications," *International Journal of Polymeric Materials and Polymeric Biomaterials* 72, no. 17 (2023): 1360–1374.

29. N. Nazeri, R. Karimi, and H. Ghanbari, "The Effect of Surface Modification of Poly-Lactide-co-Glycolide/Carbon Nanotube Nanofibrous Scaffolds by Laminin Protein on Nerve Tissue Engineering," *Journal of Biomedical Materials Research. Part A* 109, no. 2 (2021): 159–169.

30. V. Gayathri, T. Khan, M. Gowtham, R. Balan, and T. A. Sebaey, "Functionalized Conductive Polymer Composites for Tissue Engineering and Biomedical Applications – A Mini Review," *Frontiers in Bioengineering and Biotechnology* 13 (2025): 13.

31. M. Hosseinpour, G. Khalili tanha, F. Forouzanfar, M. Moghbeli, S. E. Enderami, and E. Saburi, "Application of Natural Polymers in Skin Tissue Engineering Using 3D Scaffold," *International Journal of Polymeric Materials and Polymeric Biomaterials* 74, no. 4 (2025): 285–296.

32. A. Flis, M. Trávníčková, F. Koper, et al., "Poly(Octamethylene Citrate) Modified With Glutathione as a Promising Material for Vascular Tissue Engineering," *Polymers* 15, no. 5 (2023): 1322.

33. J. Yang, A. R. Webb, and G. A. Ameer, "Novel Citric Acid-Based Biodegradable Elastomers for Tissue Engineering," *Advanced Materials* 16, no. 6 (2004): 511–516.

34. C. Han, L. Zhang, R. Bao, et al., "Biodegradable Metabotissugenic Citrate-Based Polymer Derived Self-Sealing Pro-Regenerative Membrane for Tendon Anti-Biofouling and Repair," *Bioactive Materials* 51 (2025): 598–612.

35. D. Shan, D. Wang, Y. Ma, et al., "Biodegradable Citrate-Based Polymers Enable 5D Monitoring of Implant Evolution," *Advanced Functional Materials* 35, no. 5 (2025): 2414400.

36. J. Yang, A. R. Webb, S. J. Pickerill, G. Hageman, and G. A. Ameer, "Synthesis and Evaluation of Poly(Diol Citrate) Biodegradable Elastomers," *Biomaterials* 27, no. 9 (2006): 1889–1898.

37. Y. Sun, S. Cheng, W. Lu, Y. Wang, P. Zhang, and Q. Yao, "Electrospun Fibers and Their Application in Drug Controlled Release, Biological Dressings, Tissue Repair, and Enzyme Immobilization," *RSC Advances* 9, no. 44 (2019): 25712–25729.

38. Y. Ji, K. Liang, and Y. Guo, "Fabricating Polycitrate-Based Biodegradable Elastomer Nanofibrous Mats via Electrospinning," *Journal of Elastomers and Plastics* 53, no. 3 (2021): 258–269.

39. P. Gupta, C. Elkins, T. E. Long, and G. L. Wilkes, "Electrospinning of Linear Homopolymers of Poly(Methyl Methacrylate): Exploring Relationships Between Fiber Formation, Viscosity, Molecular Weight and Concentration in a Good Solvent," *Polymer* 46, no. 13 (2005): 4799–4810.

40. L. Zhu, Y. Zhang, and Y. Ji, "Fabricating Poly(1,8-Octanediol Citrate) Elastomer Based Fibrous Mats via Electrospinning for Soft Tissue Engineering Scaffold," *Journal of Materials Science. Materials in Medicine* 28, no. 6 (2017): 93.

41. L. Vogt and A. R. Boccaccini, "Random and Aligned Electrospun Poly(ε-Caprolactone) (PCL)/poly(1,8-Octanediol-co-Citrate) (POC) Fiber Mats for Cardiac Tissue Engineering Using Benign Solvents," *European Polymer Journal* 160 (2021): 110772.

42. J. Liu, L. Argenta, M. Morykwas, and W. D. Wagner, "Properties of Single Electrospun Poly (Diol Citrate)-Collagen-Proteoglycan Nanofibers for Arterial Repair and in Applications Requiring Viscoelasticity," *Journal of Biomaterials Applications* 28, no. 5 (2014): 729–738.

43. Y. Zhang, S. Fang, J. Dai, et al., "Experimental Study of ASCs Combined With POC-PLA Patch for the Reconstruction of Full-Thickness Chest Wall Defects," *PLoS One* 12, no. 8 (2017): e0182971.

44. M. P. Prabhakaran, A. S. Nair, D. Kai, and S. Ramakrishna, "Electrospun Composite Scaffolds Containing Poly(Octanediol-co-Citrate) for Cardiac Tissue Engineering," *Biopolymers* 97, no. 7 (2012): 529–538.

45. R. Rahnamafar, F. Moradikhah, M. Doosti-Telgerd, et al., "Fine-Tuning of Hydrophilic Properties of Asymmetrically Porous Poly(ε-Caprolactone)-Based Nanofibrous Scaffolds Containing Dexamethasone for Bone Tissue Engineering Applications," *Journal of Applied Polymer Science* 142, no. 12 (2025): e56627.

46. A. Bakhtiari, H. R. Madaah Hosseini, R. Alizadeh, M. Mohammadi, and M. Zarei, "Enhancing Mechanical and Biological Properties of 3D-Printed Polylactic Acid Scaffolds by Graphitic Carbon Nitride Addition for Bone Tissue Engineering," *Journal of Materials Research and Technology* 35 (2025): 308–316.

47. C. Tommasino, C. Sardo, A. Guidone, et al., "Bioinspired PCL-Based Composite Scaffolds Produced via Hot Melt Extrusion and Fused Filament Fabrication: An Integrated Workflow for Enhanced Bone Regeneration," *Journal of Drug Delivery Science and Technology* 106 (2025): 106679.

48. F. Zou, X. Sun, and X. Wang, "Elastic, Hydrophilic and Biodegradable Poly (1,8-Octanediol-co-Citric Acid)/Polylactic Acid Nanofibrous Membranes for Potential Wound Dressing Applications," *Polymer Degradation and Stability* 166 (2019): 163–173.

49. H. Othman, E. A. Awad, S. A. Zaher, et al., "Electrospinning Process Parameters and Application: A Review," *Journal of Textiles, Coloration and Polymer Science* 22, no. 1 (2025): 59–66.

50. M. R. Almafie, A. Fudholi, R. Dani, M. K. N. A. P. Idjan, I. Royani, and I. Sriyanti, "Effects of Electrospinning Parameters on Polycaprolactone Membrane Diameter: An Investigation Utilizing Central Composite Design and Characterization," *Results in Engineering* 25 (2025): 104002.

51. F. T. Zahra, Y. Zhang, A. O. Ajayi, Q. Quick, and R. Mu, "Optimization of Electrospinning Parameters for Lower Molecular Weight Polymers: A Case Study on Polyvinylpyrrolidone," *Polymers* 16, no. 9 (2024): 1217.

52. A. Cipitria, A. Skelton, T. R. Dargaville, P. D. Dalton, and D. W. Hutmacher, "Design, Fabrication and Characterization of PCL Electrospun Scaffolds—A Review," *Journal of Materials Chemistry* 21, no. 26 (2011): 9419–9453.

53. Y. Xi, J. Ge, Y. Guo, B. Lei, and P. X. Ma, "Biomimetic Elastomeric Polypeptide-Based Nanofibrous Matrix for Overcoming Multidrug-Resistant Bacteria and Enhancing Full-Thickness Wound Healing/Skin Regeneration," *ACS Nano* 12, no. 11 (2018): 10772–10784.

54. F. Jafari, S. N. Khorasani, F. Alihosseini, D. Semnani, S. Khalili, and R. E. Neisiany, "Development of an Electrospun Scaffold for Retinal Tissue Engineering," *Polymer Science, Series B* 62, no. 3 (2020): 290–298.

55. A. Bandzerewicz, K. Wierzchowski, J. Mierzejewska, et al., "Biological Activity of Poly(1,3-Propanediol Citrate) Films and Nonwovens: Mechanical, Thermal, Antimicrobial and Cytotoxicity Studies," *Macromolecular Rapid Communications* 45, no. 2 (2024): 2300452.

56. F. Guo, K. Liang, and Y. Ji, "Electrospun Poly(Octamethylene Citrate) Thermoset Fibrous Mat From Chitin Nanocrystal Constructed Pickering Emulsion," *Colloid and Polymer Science* 302 (2024): 891–900.

57. Z. Fakhari, S. Nouri Khorasani, F. Alihosseini, M. H. Nasr Esfahani, F. Karamali, and S. Khalili, "Core–Shell Nanofibers of Poly(Glycerol Sebacate) and Poly(1,8 Octanediol Citrate) for Retinal Regeneration," *Polymer Bulletin* 79, no. 9 (2022): 7161–7176.

58. H. Vargas-Villagran, A. Romo-Uribe, E. Teran-Salgado, M. Dominguez-Diaz, and A. Flores, "Electrospun Polylactic Acid Non-Woven Mats Incorporating Silver Nanoparticles," *Polymer Bulletin* 71, no. 9 (2014): 2437–2452.

59. R. Wyrwa, B. Finke, H. Rebl, et al., "Design of Plasma Surface-Activated, Electrospun Polylactide Non-Wovens With Improved Cell Acceptance," *Advanced Engineering Materials* 13, no. 5 (2011): B165–B171.

60. K. Kowiorski, M. Heljak, A. Strojny-Nędza, et al., "Compositing Graphene Oxide With Carbon Fibers Enables Improved Dynamical Thermomechanical Behavior of Papers Produced at a Large Scale," *Carbon* 206 (2023): 26–36.

61. A. Chlanda, E. Kijeńska-Gawrońska, J. Zdunek, and W. Swieszkowski, "Internal Nanocrystalline Structure and Stiffness Alterations of Electrospun Polycaprolactone-Based Mats After Six Months of In Vitro Degradation. An Atomic Force Microscopy Assay," *Journal of the Mechanical Behavior of Biomedical Materials* 101 (2020): 103437.

62. A. N. Frone, S. Berlioz, J.-F. Chailan, and D. M. Panaitescu, "Morphology and Thermal Properties of PLA–Cellulose Nanofibers Composites," *Carbohydrate Polymers* 91, no. 1 (2013): 377–384.

63. R. Z. Khoo, H. Ismail, and W. S. Chow, "Thermal and Morphological Properties of Poly (Lactic Acid)/Nanocellulose Nanocomposites," *Procedia Chemistry* 19 (2016): 788–794.

64. A. Bandzerewicz, J. Howis, K. Wierzchowski, et al., "Exploring the Application of Poly(1,2-Ethanediol Citrate)/Polylactide Nonwovens in Cell Culturing," *Frontiers in Bioengineering and Biotechnology* 12 (2024): 1332290.